Optimization of NH2-UiO-66/TiO2/Au composites for enhanced gas-phase CO2 photocatalytic reduction into CH4

Marie Duflot, Clément Marchal, Valérie Caps, Vincent Artero, Konstantinos Christoforidis, Valérie Keller

Optimization of NH_2-UiO-66/TiO_2/Au composites for enhanced gas-phase CO_2 photocatalytic reduction into CH_4

Marie Duflot, [1] Clément Marchal, [1] Valérie Caps, [1] Vincent Artero,[2] Konstantinos Christoforidis, [3] Valérie Keller [1]*

(1) ICPEES, Institute of Chemistry and Processes for Energy, Environment and Health, CNRS/University of Strasbourg, 25 rue Becquerel 67087 Strasbourg Cedex 2, FRANCE

(2) Laboratoire de Chimie et Biologie des Métaux, CEA/CNRS/Université Grenoble Alpes, 17 rue des Martyrs, F-38054 Grenoble, Cedex, FRANCE

(3) Department of Environmental Engineering, Democritus University of Thrace, Xanthi 67100, GREECE

Corresponding author: *vkeller@unistra.fr

Abstract

Here we report on the optimization of NH_2-UiO-66/TiO_2/Au (*ca.* 1.5wt.%) composite photocatalysts applied to gas phase CO_2 photocatalytic reduction in presence of water as reducing agent by varying NH_2-UiO-66/TiO_2 ratio and pH during synthesis. It is shown that 10wt.% NH_2-UiO-66/TiO_2/Au (at pH=7) composite leads to the best cumulated CH_4 production rate of 136 µmol/$g_{catalyst}$ with 70% electronic selectivity over 5h of continuous test. This composite exhibits the best compromise between MOF surface area and thus CO_2 adsorption sites, visible light photons absorption capacity and a large interface contact area, which ensured preferable metal(Zr)-to-metal(Ti) charge carrier. Au deposition by impregnation/chemical reduction in also required to perform CO_2 photoreduction, and may presumably act as electron traps, co-catalyst or surface plasmon resonator.

Graphical abstract

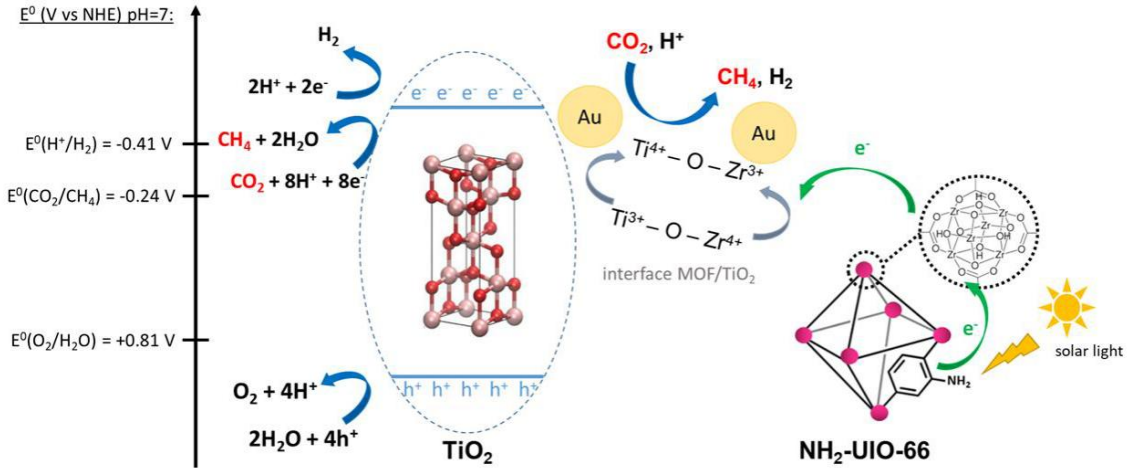

Keywords: Photocatalysis, CO_2 reduction, Titanium dioxide, MOF, NH2-UIO-66, methane

1 Introduction

The capture and the conversion of carbon dioxide CO_2 into valuable chemical fuels became a major challenge over the last few years. In the context of the ecological crisis, the reduction of greenhouse gases in the atmosphere has never been more important, in order to diminish the air pollution and contribute to slow down the global warming [1]. Beside the ecological

concern, natural energy resources (fossil fuels) continue to decrease, forcing our society to find other ways to answer the still increasing energy needs [2]. The reduction of CO_2 by photocatalysis may be a solution to produce fuels such as methane CH_4 using only solar light. Metal-organic frameworks (MOFs) have attracted a great interest especially for their capacity to trap gases. Among the different MOF structures, UiO-66 based materials have been intensively studied mostly due to their stability in a variety of conditions [3,4] and the high ability to capture CO_2. In addition to its large surface area [4,5], the functionalized MOF NH_2-UiO-66, has amine functional groups present on the organic linker allowing the efficient capture of CO_2 via chemisorption [3,6,7]. These same -NH_2 groups allow a better light harvest, absorbing in the visible range (420 nm) [8,9]. NH_2-UiO-66 has already been used for the photocatalytic reduction of CO_2 under visible light to produce CO in gas phase with a controlled flow [10], or $HCOO^-$ in liquid phase [11]. However, NH_2-UiO-66 does not present a good photocatalytic activity, particularly because of the short life time of the photogenerated electrons [12].

To increase photoactivity, MOF structures are often coupled to form heterojunctions with other semiconductors, as cadmium sulfide CdS [10,13] or titanium dioxide TiO_2 [4]. In many cases sacrificial agents such as triethanolamine have been used as electron donors [10,11]. This approach cannot be considered sustainable. TiO_2 presents high stability, has low cost and is non-toxic [14,15]. Coupling of TiO_2 with microporous networks, such as zeolite [16] or Zr-based MOFs as Zr-MOF-525 [17] and UiO-66 [18], have demonstrated the influence of porous materials to improve the photocatalytic reduction of CO_2 into CH_4.

Another interesting approach to improve photocatalytic activity is the introduction of metal nanoparticles (NPs) used as electron traps, co-catalysts, and/or allowing to induce Surface Plasmon Resonance (LSPR) properties. Au can be considered as one of the most interesting system for driving CH_4 production from CO_2 gas-phase photocatalytic reduction in the presence of water vapor [19].

The goal of this work is to couple NH_2-UiO-66 with commercially available TiO_2 to enhance its photocatalytic activity towards selective gas phase CO_2 reduction in the presence of water, into CH_4 under solar irradiation. The challenge of this study is to develop an ecological and economical pathway by using only water as reducing agent. We explored the preparation of NH_2-UiO-66/TiO_2 composites by impregnation/physical mixture method in aqueous conditions. A parametric study was focused on the influence of both pH conditions and the MOF/TiO_2 ratio. Photocatalytic tests were performed on these composite materials after deposition of low amount (≈ 1.5 wt.%) of gold nanoparticles (Au NPs), in order to enhance their photocatalytic activity for the reduction of CO_2 in humid conditions. Finally, structure/activity correlations were investigated and discussed.

2 Experimental

2.1 Catalysts synthesis

Synthesis of NH_2-UiO-66. NH_2-UiO-66 was obtained by synthesis under hydrothermal conditions [4,10]. 370 mg of zirconium chloride ($ZrCl_4$, 99.5 %, Sigma-Aldrich) with 3 mL of concentrated hydrochloric acid HCl (37%) were dissolved in 15 mL of N,N-Dimethyl Formamide (DMF, 99%) in a sonication bath for 20 min. 400 mg of 1,2-aminoterephtalic acid (ATA, 99%) dispersed in 30 mL of DMF were added. The mixture was sonicated for 20 min, transferred into a 100 mL Teflon autoclave and then heated at 150 °C during 24 h. After cooling, the solid compound was washed three times with ethanol by filtration and vacuum dried at 120 °C for 24 h.

Preparation of NH_2-UiO-66/TiO_2 P25 physical mixtures. NH_2-UiO-66 and TiO_2 P25 were coupled by physical mixture [20] in aqueous solution. Two series of samples were prepared: (i) 10%wt. NH_2-UiO-66/TiO_2 with variation of the pH and (ii) NH_2-UiO-66/TiO_2 by varying the amount of the two parts and keeping the pH constant at pH 7.
(i) For the first series 360 mg of TiO_2 were dispersed in 60 mL of H_2O in a sonication bath for 10 min, before adding 40 mg of MOF (to obtain 10%wt. of NH_2-UiO-66). The mixture was sonicated for 10 min, the pH of the solution was adjusted (pH 3, 5, 7 and 9) and let under stirring at room temperature until evaporation of the solvent. The resulting powder was dried at 100 °C for one night. (ii) For the second series 360 mg of TiO_2 were dispersed in 60 mL of H_2O in a sonication bath for 10 min, before adding a certain quantity of MOF in order to obtain mixtures with 5%wt., 10%wt. and 15%wt. of NH_2-UiO-66. The mixture was sonicated 10 min, the pH of the solution was adjusted at pH 7 and let under stirring at room temperature until evaporation of the solvent. The resulting powder was dried at 100 °C overnight.

Deposition of Au nanoparticles (NPs) was performed by impregnation/chemical reduction method [19]. 200 mg of the support were dispersed in water at room temperature, before adding an aqueous solution of tetrachloroaurate (III) hydrate ($HAuCl_4.3H_2O$, 99.99%) (0.22 M, 80 µL). After 45 min under stirring (1000 rpm), an aqueous solution of sodium tetrahydroborate ($NaBH_4$, 98%, Sigma-Aldrich) in excess ($HAuCl_4/NaBH_4$ = 1/5) was added. The mixture was let under stirring during 15 min, then filtrated and washed with 1 L of H_2O. The obtained powder was dried at 100 °C for 24 h. The nominal Au content was chosen as 1.5 %wt. The resulting samples were labelled x wt.% NH_2-UiO-66/TiO_2/Au, where x stands for the targeted content of MOF.

2.2 Characterization methods and photocatatalytic evaluation

Elemental analyses were carried out using Inductively Coupled Plasma Atomic Emission Spectroscopy (ICP-AES) to determine, the real content of Au NPs (in %wt.) in selected samples.
X-ray diffraction (XRD) patterns were obtained with a Bruker D8 Advance theta-theta diffractometer (Cu Kα radiation, λ = 0.154 nm), equipped with a LynxEye detector and operating at 40 kV and 40 mA. The datasets were acquired in step-scan mode over the 5- 90° 2θ range with a step interval of 0.005° and a counting time of 0.1 s per step.
UV-Visible absorption spectra were recorded on a Lambda 950 UV-visible spectrophotometer (Perkin Elmer) equipped with a 100 mm diffuse reflectance integrating sphere.
Nitrogen adsorption-desorption isotherms at 77 K and pores distribution were obtained using a Micrometrics Asap 2420 porosimeter. Materials were outgassed at 120 °C under primary vacuum for one night in order to eliminate water and desorb impurities from their pores. Specific surface areas were calculated by the Brunauer, Emmett and Teller (BET) method in the relative pressure (P/P_0) range 0.05-0.3 and using t-plots methods.
Transmission Electron Microscopy (TEM) was carried out on a JEOL 2100F microscope working at 200 kV accelerating voltage and equipped with a probe corrector for spherical aberrations, giving a point-to-point resolution of 0.18 nm. The samples were dispersed in an ethanol solution. A drop of the solution is then deposited on copper grid covered with a holey carbon membrane. Statistical nanoparticles size distributions are determined using the ImageJ software.
Gas-phase photocatalytic tests for the reduction of CO_2 has already been described elsewhere [19]. Typically, pure CO_2 gas is fed with a controlled flow at 0.3 $mL.min^{-1}$ through a thermo-controlled water saturator (with a maintained temperature at 30 °C). The reaction mixture

(CO_2/H_2O = 96/4) passes through a transparent photocatalytic reactor, containing the catalyst. The sample is irradiated with an artificial solar lamp (150 W Ceramic-Metal-Halide Lamp fixed at 7 cm above the reactor) (with irradiances in the 300-800 nm region: UV = 46 $W.m^{-2}$, Visible = 4271 $W.m^{-2}$) for 5 h. The gas-phase products are analyzed with on-line gas phase μGC (Agilent 3000A SRA instrument) (**Figure S1**). 45 mg of photocatalyst were suspended in ethanol and deposited onto a 50 mm diameter glass disk and let at 100 °C until dryness. The surface concentration of catalyst is around 22.5 $g.m^{-2}$. The disk was placed in the photocatalytic reactor (6 mL) and the set-up is purged with high flow of CO_2 (> 100 mL min^{-1}) to remove air, before switching on the solar lamp. Gas-phase production rates were calculated according to the following equation:

$$r_X = \frac{[x] \times 10^{-6} \times (flow\ rate) \times 60}{V_m \times m_{catalyst}}$$

where r_x is the production rate ($\mu mol.h^{-1}.g_{catalyst}^{-1}$), [x] the concentration (ppm), flow rate = 0.003 $L.min^{-1}$ and V_m = 22.4 $L.mol^{-1}$

Electronic selectivity was calculated as follows according to stoichiometry of oxido-reduction half reactions:

$$CO_2 + 2H^+ + 2e^- \rightarrow CO + H_2O \ (E^0 = -0.53\ V) \ \text{(V vs NHE, pH=7)}$$
$$2H^+ + 2e^- \rightarrow H_2 \ (E^0 = -0.41\ V)$$
$$CO_2 + 8H^+ + 8e^- \rightarrow CH_4 + 2H_2O \ (E^0 = -0.24\ V)$$
$$2H_2O + 4h^+ \rightarrow O_2 + 4H^+ \ (E^0 = +0.81\ V)$$

$$\text{Selectivity } (H_2) = \frac{2 \times \boldsymbol{r}_{H2}}{2 \times \boldsymbol{r}_{H2} + 8 \times \boldsymbol{r}_{CH4} + 2 \times \boldsymbol{r}_{CO}}$$

$$\text{Selectivity } (CH_4) = \frac{2 \times \boldsymbol{r}_{CH4}}{2 \times \boldsymbol{r}_{H2} + 8 \times \boldsymbol{r}_{CH4} + 2 \times \boldsymbol{r}_{CO}}$$

The reported reaction rates and selectivities were determined both as the average and cumulated values after 5 hours of photocatalytic test.

3 Results and discussion

3.1 Elemental analyses

The real MOF content of the composite materials is calculated from TGA analysis (**Figure S2** and **Table S1**) and shows experimental MOF content close to the nominal value (5% relative error). It can be observed that no other organic residue or moiety (other than the ones related to the MOF) is present according to published studies [4]. From ICP results, the real Au content was determined for TiO_2 P25, 15wt.% NH_2-UiO-66/TiO_2(pH=7) and 10wt.% NH_2-UiO-66/TiO_2 (pH=7) supports (**Table 1**), showing that the best deposition yield is obtained for the two former ones (90% and 87%, respectively). Increasing further the MOF content results in decreasing this yield, suggesting lower affinity and thus deposition ability onto the NH_2-UiO-66 surface.

3.2 *Structural properties of NH_2-UiO-66/TiO_2 composites*

XRD was first applied to get information on the structure of the prepared materials (**Figure 1**). A mixed phase anatase/rutile is evidenced for the pure TiO_2, typical for TiO_2 P25 [21,22]. The XRD patterns of the composites are dominated by the TiO_2 phase due to the high TiO_2 content. The major diffraction peaks of NH_2-UiO-66 centered at 2θ = 7.4° and 8.5° are detected in the composites [3,4,10]. This observation clearly suggests the presence of both phases in the composite. However, the characteristic peaks of the MOF are not detected for the composite prepared at pH 9. This suggests that NH_2-UiO-66 is not stable at basic conditions (**Figure 1b**).

In the second series where the MOF/TiO_2 ratio varied, the relative intensity of the characteristic diffraction peaks of NH_2-UiO-66 followed the content of the MOF structure in the composite (**Figure 1c**). Nevertheless, the presence of the MOF cannot be attested for 5%wt. NH_2-UiO-66/P25. It seems difficult to highlight the presence of the NH_2-UiO-66 below 10%wt. by XRD.

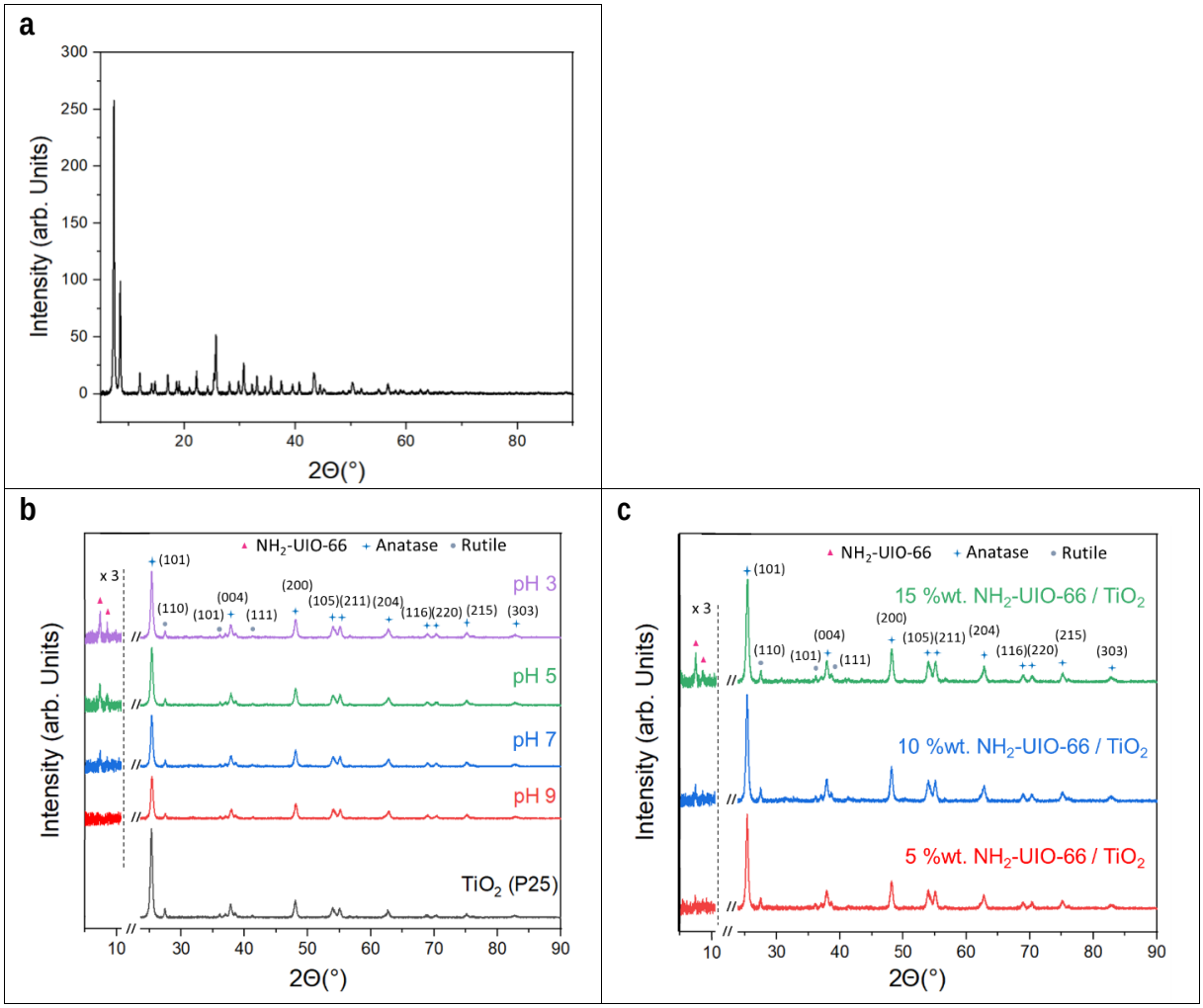

Figure 1. *XRD pattern of* ***(a)*** *NH_2-UiO-66,* ***(b)*** *10 wt.% NH_2-UiO-66/TiO_2 composites at different pH (3, 5, 7 and 9) and* ***(c)*** *NH_2-UiO-66/TiO_2 composites at pH=7 (at 5, 10 and 15wt.% MOF).*

3.3 *Surface properties and porosity of NH_2-UiO-66/TiO_2 composites*

All materials were analyzed by N_2 sorption isotherms. From **Figure 2a**, one can observe that NH_2-UiO-66 exhibits classical type-I isotherm related to micropores (maximum 2 nm) filling

at low relative pressure that can be described by Langmuir isotherm. NH_2-UiO-66 presents high specific surface area (**Table 1**). Independently of the synthesis conditions applied, the adsorption/desorption isotherm is dominated by TiO_2 features, showing type-IV This is expected due to the high content of TiO_2 in the composites **(Figure 2a and 2b)**. Focusing on the specific surface area of materials, it can be observed that the composites do not behave as physical mixtures since their specific surface area cannot be reproduces simply by linear combination of their constituents **(Table 1)** (except for 10 wt.% NH_2-UiO-66/P25, pH=3). This may suggest the formation of intra-granular mesoporosity probably through the formation of an interface between the TiO_2/MOF phases developed during synthesis. This is supported by the larger mesoporous volume in the composite materials than the reference TiO_2 (**Figure 2c and 2d**).

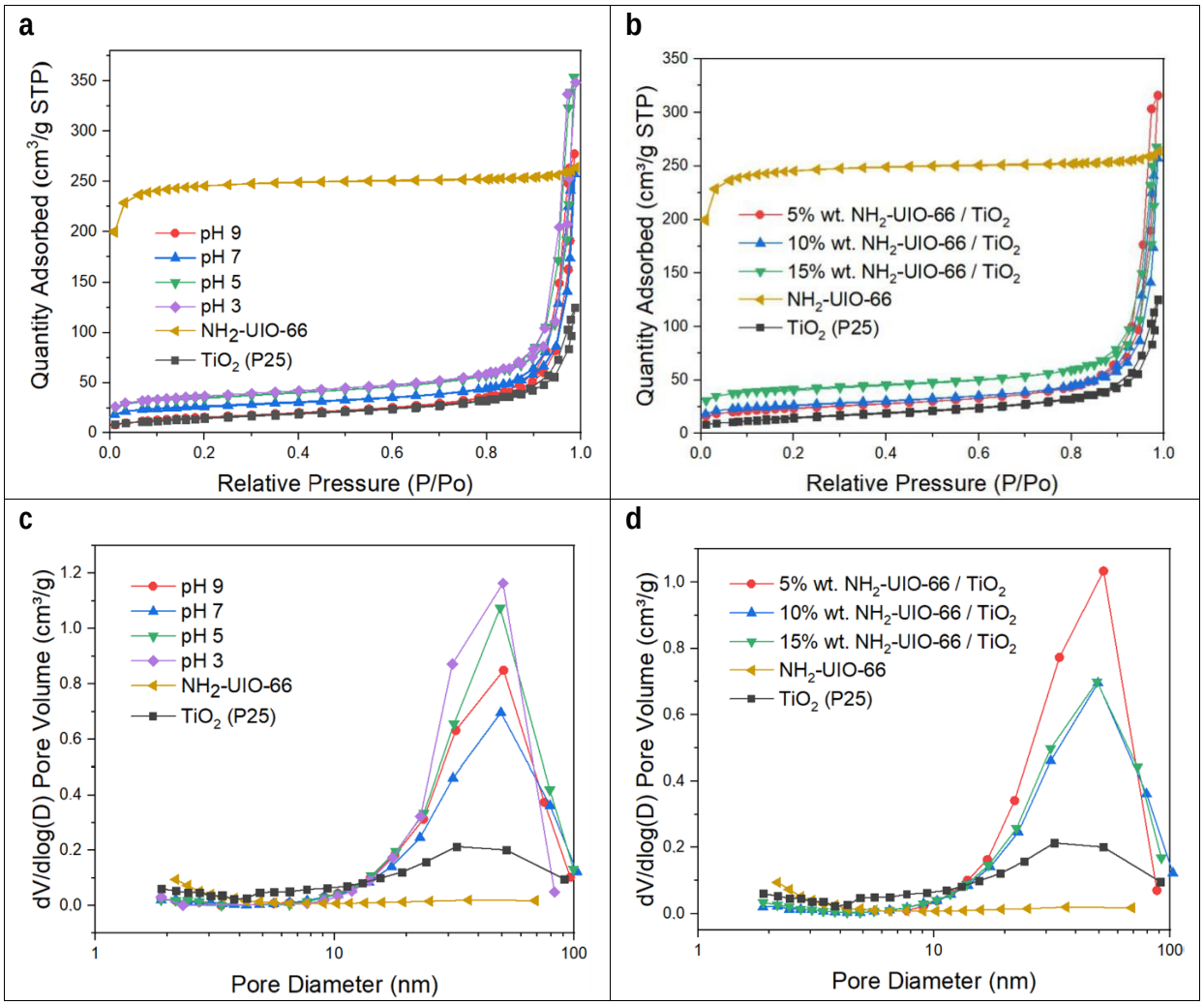

Figure 2. *N_2 adsorption/desorption isotherms of* ***(a)*** *10 wt.% NH_2-UiO-66/TiO_2 composites at different pH (3, 5, 7 and 9) and* ***(b)*** *NH_2-UiO-66/TiO_2 composites at pH=7 (at 5, 10 and 15wt.% MOF).*
Porous distribution of ***(c)*** *10 wt.% NH_2-UiO-66/TiO_2 compositse at different pH (3, 5, 7 and 9) and* ***(d)*** *NH_2-UiO-66/TiO_2 composites at pH=7(at 5, 10 and 15wt.% MOF).*

Table 1. *Surface area, pore volume and diameter, experimental Au loading and deposition yield.*

Samples	S_{BET} (m^2/g)	V pores (cm^3/g)*	Average pore diameter (nm)*	Au loading, wt.% (Deposition yield, %)**
TiO_2 P25	53 ± 5	0.19	48	1.44 ± 0.04 (90)
NH_2-UiO-66	806 ± 50	0.07	2	
10 wt.% NH_2-UiO-66/P25 (**pH=9**)	58 ± 5	0.43	51	
10 wt.% NH_2-UiO-66/P25 (**pH=7**)	90 ± 7	0.38	49	1.09 ± 0.02 (68)
10 wt.% NH_2-UiO-66/P25 (**pH=5**)	119 ± 8	0.52	49	
10 wt.% NH_2-UiO-66/P25 (**pH=3**)	128 ± 9	0.51	51	
5 wt.% NH_2-UiO-66/P25 (**pH=7**)	82 ± 7	0.48	52	
15 wt.% NH_2-UiO-66/P25 (**pH=7**)	139 ± 10	0.38	49	1.39 ± 0.03 (87)

**Experimental error of 6%. **Determined from ICP.*

3.4 Optoelectronic properties of UiO-66/TiO_2 composites

UV-Vis absorbance measurements of the different composite materials **(Figure 3a and 3c)** show three main contributions: (i) the one for the commercial TiO_2 P25; (ii) the one assigned to NH_2-UiO-66 MOF related to photoinduced electron transfer from 2-aminoteraphtalate linkers to Zr-oxo clusters and consistent with previous reports [5,11]; (iii) a third displaying absorption at longer wavelengths compared with pure TiO_2 and NH_2-UiO-66. This redshift of NH_2-UiO-66/TiO_2 composites could be attributed to a favorable Ti^{4+}-mediated photoinduced electron transfer, from excited 2-aminoteraphtalate moieties to Zr-O-clusters, as Ti atoms might have a significant contribution to the LUMO of NH_2-UiO-66 MOF [5].
In our case, this effect is the most pronounced when preparation takes place at pH≥5 for materials containing 10 wt.% of the MOF. One may assume that in these experimental conditions NH_2-UiO-66 and TiO_2 particles exhibit the most favorable quality of interface. On the resulting materials, the composite catalyst can absorb more visible light, which

consequently may generate more photogenerated carriers. Similar phenomenon have been observed in other MOF-based photocatalysts [11]. The HOMO-LUMO gap value of NH_2-UiO-66 and band gap value of TiO_2, estimated by the Kubelka-Munk function are measured to be 2.6 and 3.2 eV.

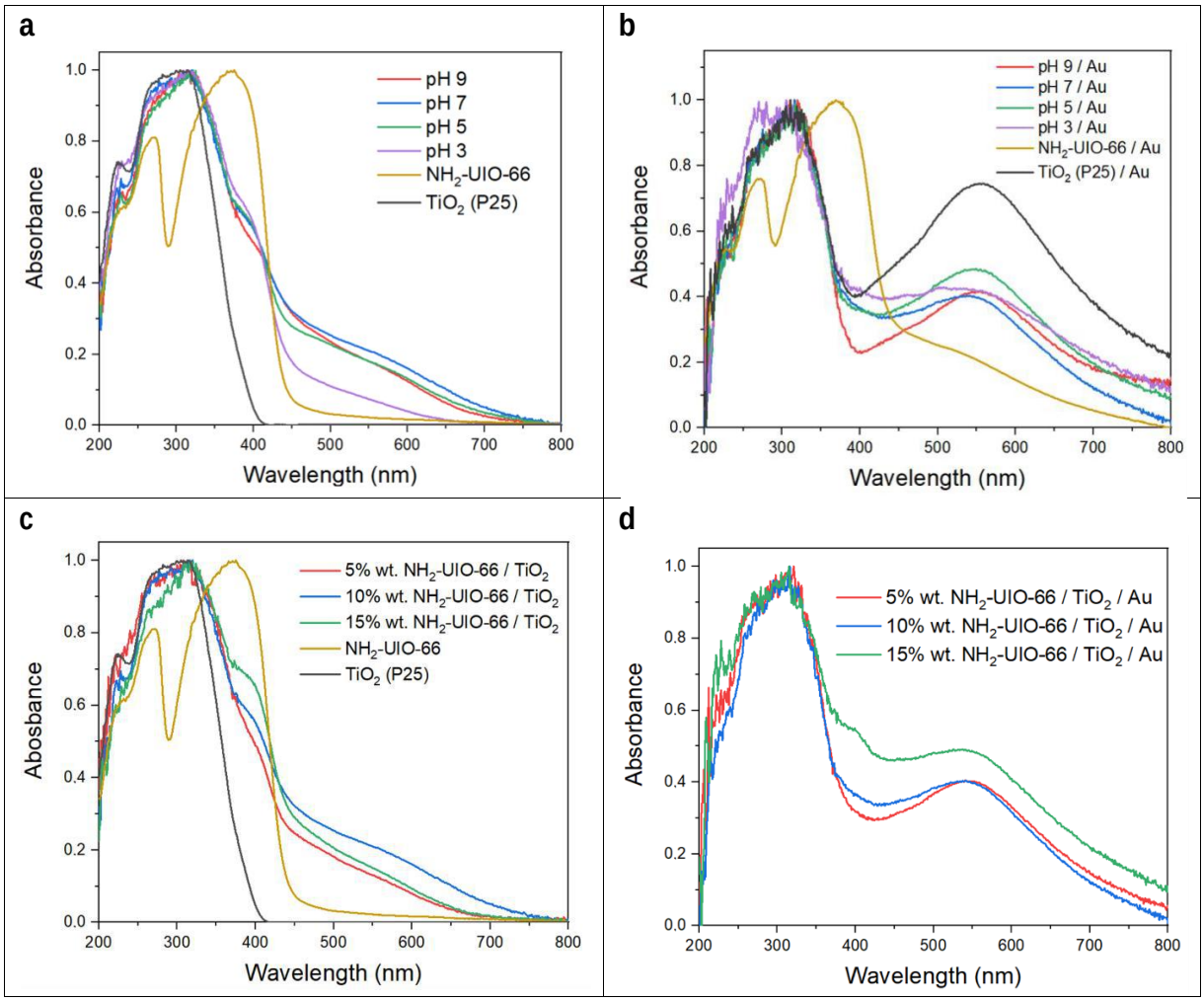

Figure 3. *UV-Visible absorbance spectra of 10 wt.% NH_2-UiO-66/TiO_2 composites at different pH (3, 5, 7 and 9)* ***(a)*** *without and* ***(b)*** *with Au deposition and of NH_2-UiO-66/TiO_2composites at pH=7 (5, 10 and 15wt.% MOF) g* ***(c)*** *without and* ***(d)*** *with Au deposition.*

After Au deposition **(Figure 3b and 3d)**, absorption in the visible range is significantly enhanced. The significant feature centered at *ca.* 550 nm is attributed to the localized surface plasmon resonance of Au NPs [23]. The position of the LSPR signal is typical of spherical Au NPs in interaction with titania [24]. The unchanged position of the LSPR signal suggests that Au NPs have a similar spherical shape in all samples, regardless of the MOF content, as further confirmed by TEM observation of 10 wt.% NH_2-UiO-66/TiO_2/Au and TiO_2/Au **(Figure S3)**. However, the intensity and full width at half maximum (FWHM) of the LSPR signals vary from one sample to another. This may be attributed to different Au particle size, content and distribution over the support. Looking at Au mean particles size deposited onto TiO_2 P25 and 10 wt.% NH_2-UiO-66/TiO2 P25 supports, TEM images **(Figure S3)** reveal that the distribution is narrower and centered onto smaller particles (3 nm *vs* 4.6 nm) in the MOF-free sample. Consequently, the more intense LSPR signal of TiO_2/Au may be attributed to the highest Au content (as evidenced by ICP, see Table 1) but also to the narrower size distribution of well-distributed individual, isolated Au NPs. The larger Au NPs size distribution observed on the MOF-containing composite suggests that the MOF disturbs the

Au NP size control that can be achieved by this synthesis method over titania and that Au NPs are more aggregated on the MOF-containing composites. Furthermore, from **Figure S3**, one can notice that Au NPs are quite exclusively deposited on TiO_2 surfaces and scarcely on the MOF. However, one can observe a MOF/TiO_2 interface for the MOF-containing composite (**Figure S3b**) with the presence of Au NPs on it.

3.5 *Photocatalytic evaluation of NH_2-UiO-66/TiO_2 composites*

Preliminary blank experiments have been conducted under Argon (without any CO_2) to make sure that that carbon-based products are from the CO_2 introduced in the reactor and not from any other carbon residue.

Figure 4 displays the photocatalytic CO_2 reduction results in the gas phase, using water as reductant under simulated sun-light. Only CH_4 and H_2 were detected as products in the gas phase. The first observation is that no detectable photocatalytic activity was evidenced over NH_2-UiO-66/Au material. Some preliminary tests without Au NPs did not reveal any significant activity. However, after Au deposition all composites developed presented higher photoactivity and selectivity towards CH_4 compared with TiO_2 alone. As evidenced, the pH value of the synthesis mixture has great effect on activity. pH=9 is detrimental presumably due to the instability of NH_2-UiO-66 at basic conditions. The composite prepared at pH 7 presented superior activity (**Figure 4a and 4b**).

In addition, the content of the MOF in the composite affected also activity (**Figure 4c and 4d).** One can clearly observe that the 10% NH_2-UiO-66/TiO_2/Au photocatalyst exhibits the best performance regarding CH_4 reaction rate. The rate of production in function of time under irradiation of this sample were obtained (**Figure S4**). It is also worthy to underline that coupling NH_2-UiO-66 with TiO_2 results in increased selectivity towards CH_4 formation from 47 to 70 % (for MOF loading > 5wt.% and pH < 9). Focusing on the specific reaction rates, normalized by the surface area, the same trend of activity is observed. This is probably linked with the moderate changes on specific surface area observed for the active composites prepared at pH 3-7.

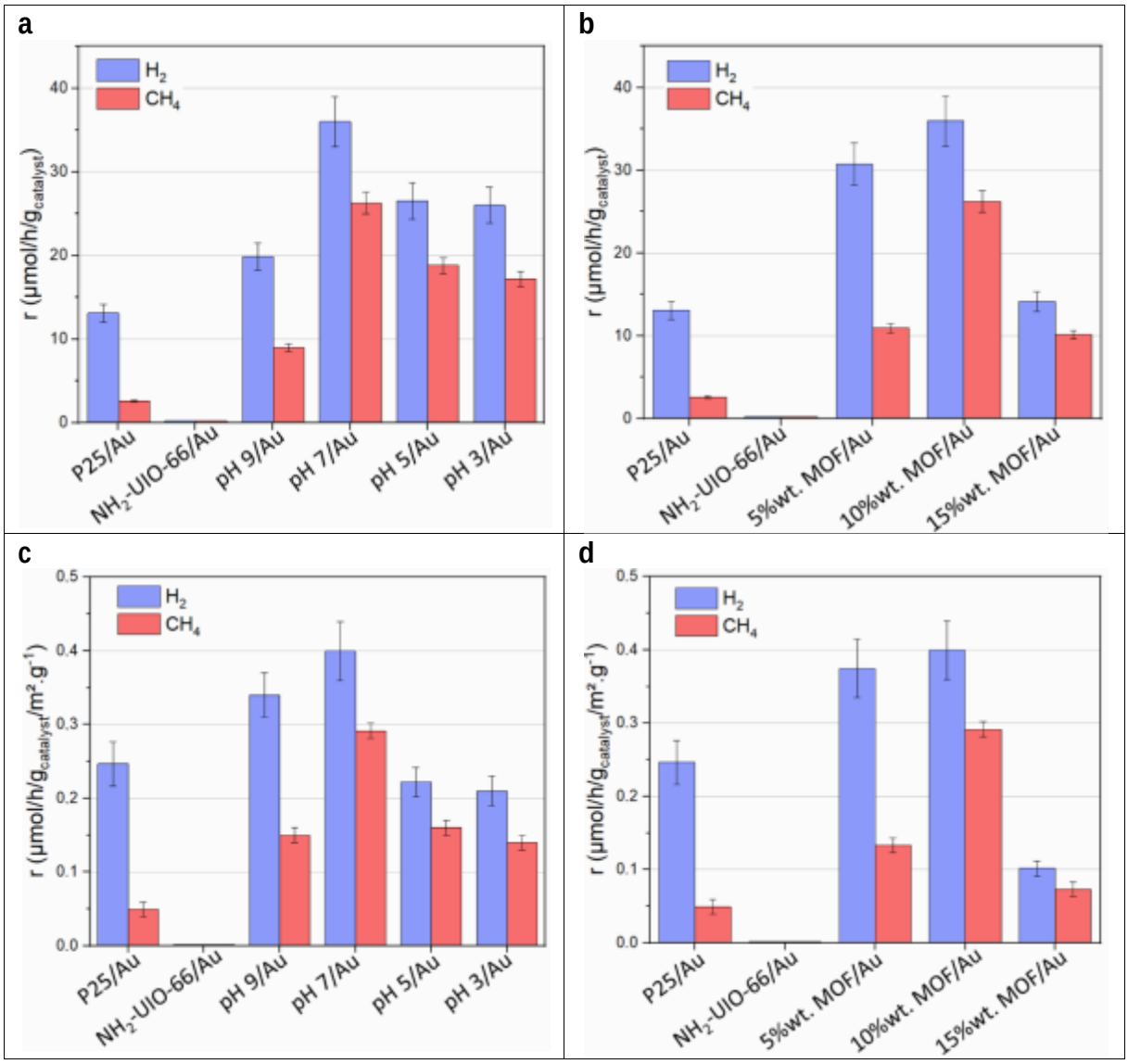

Figure 4. *Specific H_2 (blue) and CH_4 (red) average production rate in presence of water vapor (during 5 h) under continuous CO_2 flow (0.3 mL/min) and under solar light irradiation on* ***(a)*** *10 wt.% NH_2-UiO-66/TiO_2 composites at different pH (3, 5, 7 and 9) and* ***(b)*** *NH_2-UiO-66/TiO_2 composites at pH=7 (at 5, 10 and 15wt.% MOF), and average production rate in function of S_{BET} on* ***(c)*** *10 wt.% NH_2-UiO-66/TiO_2 composite at different pH (3, 5, 7 and 9) and* ***(d)*** *NH_2-UiO-66/TiO_2 composites at pH=7 (at 5, 10 and 15wt.% MOF).*

Table 2. *Average rate of production and cumulated production, and electronic selectivity over 5h of test.*

Samples	Average rate of production (µmol/h/$g_{catalyst}$)		Cumulated production in 5h (µmol/$g_{catalyst}$)		Electronic selectivity (%)		
	H_2	**CH_4**	**H_2**	**CH_4**	**H_2**	**CH_4**	**CO**
TiO_2 P25/Au	13.0	2.5	68.0	13.0	51	47	2
NH_2-UiO-66/Au	n.d	n.d	n.d	n.d	n.d	n.d	n.d
10 wt.% NH_2-UiO-66/ TiO_2 (**pH=9**)/Au	20.0	9.0	120.0	49.0	36	58	6
10 wt.% NH_2-UiO-66/ TiO_2 (**pH=7**)/Au	36.0	26.0	185.0	136.0	25	70	5
10 wt.% NH_2-UiO-66/ TiO_2 (**pH=5**)/Au	26.5	18.5	137.0	97.0	24	70	6
10 wt.% NH_2-UiO-66/ TiO_2 (**pH=3**)/Au	26.0	17.0	134.0	89.0	28	68	4
5 wt.% NH_2-UiO-66/ TiO_2 (**pH=7**)/Au	30.8	11.0	158.0	56.0	44	56	0
15 wt.% NH_2-UiO-66/ TiO_2 (**pH=7**)/Au	12.3	9.0	64.0	46.0	24	70	6

From all the previously mentioned characterization results, correlated with photocatalytic activity, one can suggest the general charge carrier and reaction pathway scheme illustrated in **Figure 5**. Upon irradiation ligand-to-metal charge transfer is expected within the MOF structure, from photoexcited organic linker to metal oxo-cluster. Based on the band structure of TiO_2 and NH_2-UIO-66 [4], electrons are expected to move from NH_2-UIO-66 to TiO_2 interface [5]. CO_2 reduction takes place on the TiO_2 part, where the presence of Au NPs would enhance the photocatalytic activity. Therefore, TiO_2 would be the active part where CO_2 reduction takes place. This can explain the inability to detect any reaction products in the NH_2-UiO-66/Au sample. The suggested mechanism may improve charge availability.

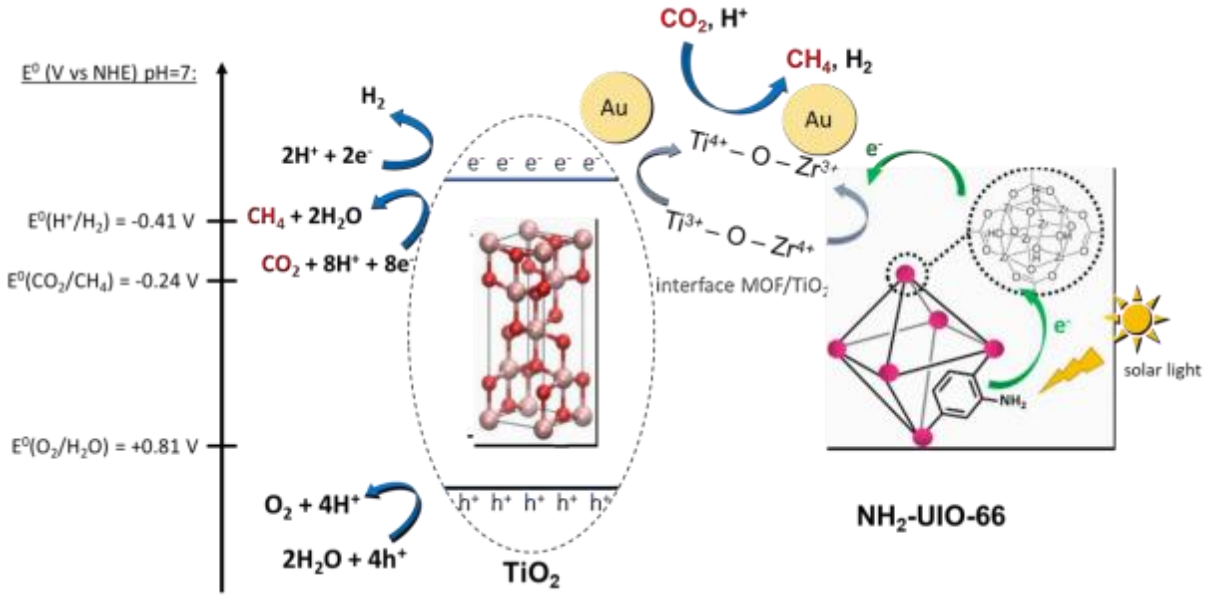

Figure 5. *Schematic charge carrier and reaction pathways on NH_2-UiO-66/TiO_2 composites.*

4 Conclusion

In the present study a facile synthesis protocol was developed and optimized for the development of NH_2-UiO-66/TiO_2/Au composites with improved activity and selectivity towards CO_2 reduction into CH_4. It is shown that optimized 10wt.% NH_2-UiO-66/TiO_2/Au composite exhibits the best compromise between MOF surface area and thus CO_2 adsorption sites, visible light photons absorption capacity and a large interface contact area, which ensured preferable metal(Zr)-to-metal(Ti) charge carrier. Furthermore, Au NPs may also play the role of electron traps, CO_2 reduction co-catalyst and surface plasmon resonator. The study highlights the importance of both the MOF content but, most importantly, the effect of the pH of the mixture during the synthesis of the composite on photoactivity and selectivity.

Acknowledgements

The project is financially supported by la Direction Générale Déléguée à la Science du CNRS. This work was also partly supported by the Agence Nationale de la Recherche (Labex ARCANE, CBH-EUR-GS, ANR-17-EURE-0003).
Financial support from the French National Research Agency (ANR) under the Program "Make Our Planet Great Again" (ANR-18-MOPGA-0014) is fully acknowledged too.

References

[1] L. Gatti, L. Basso, J. Miller, M. Gloor, L. Dominigues, H. Cassol, G. Tejada, L. Aragão, C. Nobre, W. Peters, L. Marani, E. Arai, A. Sanches, S. Corrêa, L. Anderson, C. Von Randow, C. Correia, S. Crispim, R. Neves, Nature, vol. 595, (2021), 388–393.
[2] K. Yoro, M. Daramola, Advance in Carbon Capture, in: CO2 emission sources, greenhouse gases, and the global warming effect, (2020), 3-28.
[3] A. Crake, K. Christoforidis, A. Gregg, B. Moss, A. Kafizas, C. Petit, Small (2019) 1805473.
[4] A. Crake, K. Christoforidis, A. Kafizas, S. Zafeiratos, C. Petit, Applied Catalysis B: Environmental, 210 (2017) 131–140.
[5] A. Santiago Portillo, H. Baldoví, M. García Fernandez, S. Navalon, P. Atienzar, B. Ferrer, M. Alvaro, H. Garcia Z. Li, J. Phys. Chem. C, 121 (2017) 7015–7024.
[6] X. Wang, X. Zhao, D. Zhang, G. Li, H. Li, Applied Catalysis B: Environmental, 228 (2018), 47–53.
[7] B. Arstad, H. Fjellvåg, K. O. Kongshaug, O. Swang, R. Blom, Adsorption, 14 (2008), 755–762.
[8] D. Sun, W. Liu, M. Qiu, Y. Zhang, Z. Li, Chem. Commun. , 51 (2015), 2056–2059.
[9] C. Gomes Silva, I. Luz, F. X. Llabrés i Xamena, A. Corma, H. García, Chem. Eur. J., 16 (2010), 11133–11138.
[10] X. Xie, X. Dao, F. Guo, X. Zhang, F. Wang, W. Sun, ChemistrySelect, vol. 5 (2020), 4001–4007.
[11] D. Sun, Y. Fu, W. Liu, L. Ye, D. Wang, L. Yang, X. Fu, Z. Li, Chem. Eur. J., 19 (2013), 14279–14285.
[12] M. Nasalevich, C. Hendon, J. Santaclara, K. Svane, B. van der Linden, S. Veber, M. Fedin, A. Houtepen, M. van der Veen, F. Kapteijn, A. Walsh, J. Gascon, Sci Rep, 6 (2016), 23676-23684.

[13] H. Yang, C. Yang, N. Zhang, K. Mo, Q. Li, K. Lv, J. Fan, L. Wen, Appl. Catal. B. 285 (2021), 119801.
[14] N.M. Dimitrijevic, B.K. Vijayan, O.G. Poluektov, T. Rajh, K.A. Gray, H. He P. Zapol, J. Am. Chem. Soc., 133 (2011), 3964–3971.
[15] L. Liu, Y. Li, Aerosol Air Qual. Res., 14 (2014), 453–469.
[16] M. Anpo, H. Yamashita, Y. Ichihashi, Y. Fujii, M. Honda, J. Phys. Chem. B, 101 (1997), 2632–2636.
[17] W. Gao, H.T. Ngo, Z. Niu, W. Zhang, Y. Pan, Z. Yang, V.R. Bhethanabotla, B. Joseph, B. Aguila, S. Ma, ChemSusChem, 10.1002/cssc.202001610.
[18] Y. Ma, Q. Tanga, W. Sunb, Z. Yaob, W. Zhuc, T. Lia, J. Wang, Applied Catalysis B: Environmental, 270 (2020), 118856-118864.
[19] S. Bardey, A. Bonduelle-Skrzypczak, A. Fécant, Z. Cui, C. Colbeau-Justin, V. Caps, V. Keller, Faraday Discuss., 214 (2019), 417–439.
[20] J. Zhang, Y. Hu, J. Qin, Z. Yang, M. Fu, Chemical Engineering Journal, 385 (2020) 123814-.
[21] L.A. González-Burciaga, C.M. Núñez-Núñez, M.M. Morones-Esquivel, M. Avila-Santos, A. Lemus-Santana, J.B. Proal-Nájera, Catalysts, 10 (2020), 118-128.
[22] M. Shaban, J. Poostforooshan, A. P. Weber, J. Mater. Chem. A, 5 (2017),18651–18663.
[23] L. Hammoud, C. Strebler, J. Toufaily, T. Hamieh, V. Keller V. Caps, Faraday Discuss. (2022).
[24] C. Marchal, A. Piquet, M. Behr, T. Cottineau, V. Papaefthimiou, V. Keller, V. Caps, J. Catal. 352 (2017) 22-34

CRediT authorship contribution statement

Marie Duflot: Synthesis, Characterizations, Assessment of photocatalytic activity. **Clément Marchal**: Contribution to photocatalytic test evolution. **Valérie Caps**: Contribution to the optimization of gold nanoparticles deposition. **Vincent Artero**: Collaborator, Contribution to the overall discussion. **Konstantinos Christoforidis**: Collaborator, Contribution to the overall discussion. **Valérie Keller**: Supervision of the project.